Experimental Verification of a Micrometeoroid Damage in the PN-CCD Camera System aboard XMM-Newton

Norbert Meidinger[a,*], Bernd Aschenbach[a], Heinrich Bräuninger[a], Gerhard Drolshagen[b], Jakob Englhauser[a], Robert Hartmann[c], Gisela Hartner[a], Ralf Srama[d], Lothar Strüder[a], Martin Stübig[d], and Joachim Trümper[a]

[a] Max-Planck-Institut für extraterrestrische Physik, Giessenbachstrasse, 85741 Garching, Germany
[b] ESA/ESTEC, Postbus 299, 2200 AG Noordwijk, The Netherlands
[c] PNSensor GmbH, Römerstrasse 28, 80803 München, Germany
[d] Max-Planck-Institut für Kernphysik, Saupfercheckweg 1, 69117 Heidelberg, Germany

ABSTRACT

The pn-CCD is the focal plane detector of one of the three X-ray telescopes aboard the XMM-Newton observatory. During revolution #156 more than 30 individual bright pixels lightened up out of approximately 150,000 pixels of the 6 cm x 6 cm large detector area. The amount of leakage current generated in the pixels cannot be explained by single heavy ions impact, however. We suggest that a micrometeoroid scattered off the mirror surface under grazing incidence reached the focal plane detector and produced the bright pixels. This proposal was studied by us experimentally at the Heidelberg dust accelerator. Micron-sized iron particles were accelerated to speeds of the order of 5 km/s impinging on the surface of an X-ray mirror under grazing incidence. Scatter products have been found with detectors placed behind the mirror. They have been analyzed by various methods to characterize their properties and the effects produced by them in the pn-CCD. Micrometeoroid damage to semiconductor detectors in the focus of grazing incidence optics might be of concern for future space projects with very large collecting area and are proposed to be studied in detail.

Keywords: Dust accelerator, grazing incidence, micrometeoroid, pn-CCD, XMM-Newton, X-ray mirror

1. INTRODUCTION

The XMM-Newton observatory was successfully launched on December 10, 1999.[1] The X-ray optics consists of three X-ray telescopes with unprecedentedly large effective areas. The on-axis effective area of one telescope is about 1500 cm^2 for an X-ray energy of 1 keV. Each mirror module is composed of 58 Wolter I mirror shells nested in a coaxial and confocal configuration. The focal length of the telescope is 7.5 m. A thin gold layer is used as reflective coating on nickel as mirror substrate material. The circular field of view extends to 30 arcmin in diameter which corresponds to 65.5 mm in the focal plane.

One focal plane camera is placed in the focus of each telescope. It is equipped with a high resolution scientific CCD specially developed for the XMM-Newton mission. Two of the imaging spectrometers use MOS-CCD arrays, while the third one applies a pn-CCD.[2] All three cameras together are called European Photon Imaging Camera (EPIC) taking images and spectra of the X-ray sources focused by the three telescopes.

The in-orbit commissioning of the instruments was completed in March 2000. The pn-CCD camera operated in orbit as calibrated on ground. The instrument performance was stable in time showing no radiation damage[3] besides a slight and expected CTI increase for all pixels with a long-term trend of about 1.5×10^{-5} per year (measured for the Mn-K_α-line).[4]

* Correspondence: E-mail: nom@hll.mpg.de

During the observation of Zeta Puppis in revolution #156 a sudden increase of the event rate occurred.[5] The observatory was at that time in a distance of 115,000 km from the earth and the camera was operated in large window mode with the medium thick optical filter placed in front of the detector. The angle between flight and observing direction was 60º in the heliocentric coordinate system. The rise in the event rate was so high that it caused a loss of data.

The increase was caused by a simultaneous formation of about 35 bright pixels randomly distributed over six of the in total twelve CCD units (see Fig.1). The maximum distance between the bright pixels corresponds to about 20 arcmin. Bright pixel in this context means that the event threshold is frequently (at least in every tenth frame) exceeded by the noise signal which is due to a high dark current. It took up to a few days until the dark current of some bright pixels has reached a stable value. The appearance of the bright pixels persists up to date. For a measurement of the generation current which accumulates in the affected pixels, the pn-CCD was operated in the low gain mode. This allows for an extension of the dynamic range of the energy detection. The current ranged up to more than 10^{-13} A for the most severely damaged pixels. This means an increase by several orders of magnitude in proportion to the values measured before the event had happened. This was measured at the regular operating temperature of the detector of -90ºC. A current increase expected as a result of the damage due to heavy ions impact would be smaller by several orders of magnitude than what we had found.[5] While the pixels lightened up in the pn-CCD, no unusual effect was observed at the same time in the two EPIC MOS-CCD cameras.

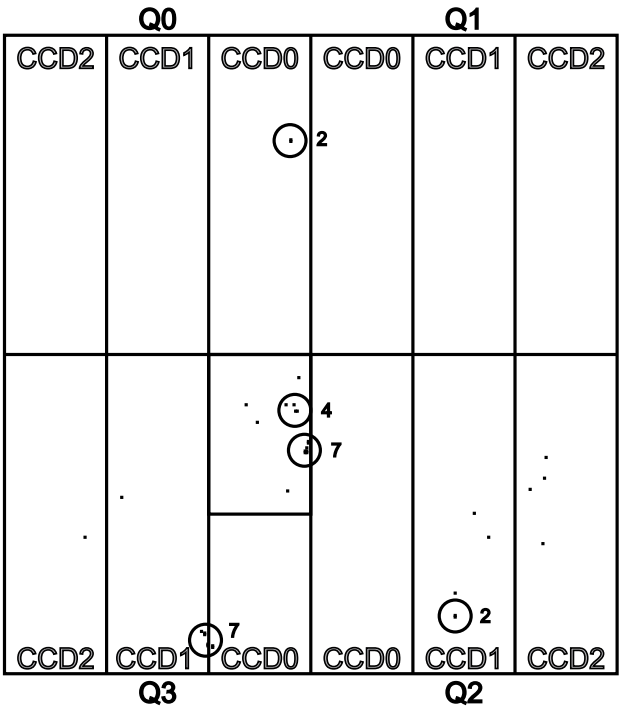

Figure 1: Pattern of bright pixel distribution after the event had occurred in the pn-CCD camera on the XMM-Newton observatory during revolution #156. The 35 bright pixels are distributed over six of the in total twelve CCD units within a distance of more than 20 arcmin. Each CCD unit has a size of 3 cm x 1 cm, the total area of the whole CCD array is 6 cm x 6 cm comprising about 150,000 pixels. The area which comprises the most damage is found in CCD0 of quadrant Q3. If bright pixels are close together they are encircled in the figure for clearness and the number of enclosed bright pixels is denoted. The focal point of the X-ray telescope is located in the lower third of CCD0 in quadrant Q1.

Similar events had happened previously during revolution #107 in the MOS2 camera and later on in the MOS1 camera during revolution #325. In the MOS1 camera again more than 20 bright pixels were simultaneously generated, distributed over an area of a few hundred times a few hundred pixels while no unusual effects were observed in the other two focal plane cameras on XMM-Newton. The event was accompanied by a diffuse “light flash” which could be observed in the image (with an exposure time of 2.6 s) taken at the time when the bright pixels started to lighten up. The maximum light intensity was coinciding with the locations of the bright pixels.[6]

The observed characteristics of the damage events which are the simultaneous formation of many bright pixels, their wide distribution over the detector area, the magnitude of the dark current, the restriction of the event to only one of three cameras and finally the occurrence of a “light flash” cannot be explained by usual kinds of radiation damage.

The suspicion emerged that the observed damage could be caused by a micrometeoroid. A straight path through the mirror system is not possible due to the paraboloid and hyperboloid shape and the tight nesting of the mirror shells. We suggested that the micrometoroid impinged under grazing incidence on the gold coated mirror surface and then generated scatter particles which finally reached the focal plane detector.[5]

We can think about different scenarios how the scatter particles were generated. The micrometeoroid may stick in the 2000 Å thick gold layer of the mirror surface and lead to a forward ejection of gold particles. Another possibility is that the dust particle breaks up when it impinges on the mirror and its fragments are scattered in forward direction. A third alternative suggestion could be that the micrometeoroid is scattered through the mirror shells and produces ejecta in the optical filter foil in front of the CCD detector.

An experimental study was performed about the interaction of dust particles with an X-ray mirror surface under grazing incidence condition.

2. EXPERIMENTS AT THE DUST ACCELERATOR

The dust accelerator at the Max-Planck-Institut für Kernphysik in Heidelberg provides micron-sized particles as projectiles for hypervelocity impact experiments. The facility is typically used to test the effect of cosmic dust impinging under perpendicular incidence angles to instruments for space applications. The effect of a dust particle interacting under grazing incidence with an X-ray mirror surface has not been studied yet in an experiment as far as we know. In our tests single dust particles were accelerated to a plane X-ray mirror under different grazing incidence angles. The detection and the properties of generated scatter particles were studied in different experiments. The experimental set-ups are described below.

2.1 Dust accelerator

An electrostatic Van-de-Graaff generator provides the acceleration voltage U_{acc} of 2 MV for positively charged particles from a dust powder source. The accelerated particle passes through a double shielded tube of 0.28 m length which is connected to a charge sensitive preamplifier. Thereby the charge q of the particle is induced on the tube and can be calculated from the signal height with known amplifier sensitivity. The particle speed v is measured by the flight time through the tube which is given by the signal pulse length. The mass m of the particle results from the energy conservation law: $1/2\ m\ v^2 = q\ U_{acc}$. For particles of spherical shape with a homogeneous mass density ρ the particle radius r can be calculated from: $4/3\ \pi\ r^3 = m/\rho$. The charge q, the speed v, the mass m and the diameter 2 r of every dust particle leaving the particle parameter selection unit (PSU) is analyzed and registered. An important feature of the Heidelberg dust accelerator is the possibility to trigger single particles manually so that it is ensured that detected scatter particles are due to the impact of one dust particle only. If a high particle rate is required for statistical reasons, a continuous auto-mode can be chosen.

With the PSU also a speed window can be set. If an accelerated dust particle does not meet the speed constraint it is deflected. A description of the Heidelberg dust accelerator and an overview of dust particle materials available can be found in Stübig et al.[7]

We chose iron particles as projectiles for our experiment with speeds in the mean range of 1 km/s to 10 km/s where the dust accelerator is most efficient. The typical positive charge on the particles ranged between 10^{-13} C and 10^{-14} C. The mass of these particles is in the order of 10^{-16} kg up to 10^{-13} kg with a diameter in the range between 0.2 µm and 2 µm.

2.2 Scatter chamber

The selected particles entered the scatter chamber through a tube which acted as an aperture. The angular distribution of the dust particles which passed through both tubes, that of the dust accelerator and that in the scatter chamber, was smaller than ±0.2º.

A plane gold coated X-ray mirror disk was placed behind the tube. The mirror substrate material Zerodur is covered by 40 Å of copper and 3000 Å of gold. The mirror could be tilted with respect to the direction of the incident dust particles to enable different grazing incidence angles. The set-up offered the option to move the mirror laterally out of the particle path so that the effect of direct dust particle impingement could be tested. Both, the tube and the mirror were connected with charge sensitive amplifers for signal detection. Thus we could check that the particle passed through the tube and then impinged on the mirror.

The set-ups for the analysis of scatter particles resulting from the interaction between the dust particle and the mirror surface were placed behind the mirror. To allow measurements at different scatter angles, the set-ups could be rotated around the mirror. They were equipped with a mechanism for an accurate measurement of the rotation angle with respect to the mirror surface. The three different detection systems for scatter particles and their purposes are described in the next three sections.

2.2.1 Scatter particle occurrence, speed and charge

A second tube and a copper target were mounted in the scatter chamber behind the mirror as shown in Fig. 2. Both were connected to charge sensitive amplifiers. Scatter particles passing through the tube induce a signal, like the dust particles do in the first tube in the chamber, proportional to the charge they carry. The tube acted also as aperture to confine the scatter angle to a region of 0.88º and by the use of a tube insert to only 0.44º respectively. If a scatter particle travels through the tube it is stopped in a copper target. A positive bias voltage is applied to the target in order to attract the electrons generated due to the particle impact, and to repel positive charge carriers. Thus we obtain a distinctive impact signal.

When a single dust particle is triggered, the signals of the first tube, the mirror, the second tube and the target are recorded with a 4-channel digital storage oscilloscope and analyzed afterwards. The shape of the signal in the first tube provides the information whether the dust particle has passed through the tube and gives the opportunity for a cross-check determination of speed and charge of the dust particle as measured before in the long tube of the PSU. The signal of the mirror shows that the dust particle has hit the mirror and at which time the impact occurred.

If a signal is observed in the second tube, its shape reveals again whether the particle has passed through the unit or impinged on it. In the case of passage, the sign of the signal indicates whether the scatter particle carries a positive or negative charge and the height of the induced signal measures the amount of charge.

In the event that the scatter particle travels through the second tube it impinges on the copper target and causes a signal indicating the hit. This method ensures that also uncharged or only slightly charged scatter particles will be detected.

The speed of the scatter particles can be calculated by the distance between mirror and copper target and the difference in time between the corresponding signals.

The alignment of the entire experimental set-up was accomplished by means of dust particles with the mirror moved out of the chamber center. The zero degree setting was attained when the dust particles passed through the center of both tubes and hit the copper target.

The probability for the occurrence of scatter particles in dependence on the grazing incidence angle of the dust particle and the scatter angle was measured in several test series. The tilt angle of the mirror with respect to incident particles was varied in four steps: 1.0º, 1.5º, 2.0º and 4.0º. Each of these mirror positions was checked for the incidence of scatter particles by rotating the second tube and the target step by step. The results are presented in section 3.1.

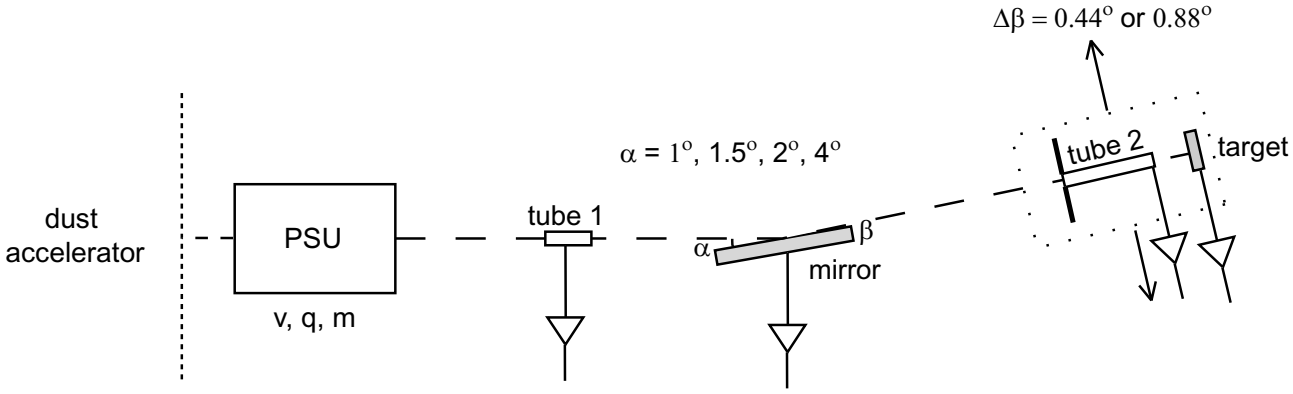

Figure 2. Experimental set-up at the dust accelerator for the detection of scatter particles caused by a dust particle which impinges on the mirror under grazing incidence. The speed v, charge q and mass m of the dust particle leaving the dust acclerator were measured with the PSU. Four different grazing incidence angles α have been tested by rotating tube 2 together with the target around the mirror step by step. The probability of scatter particle occurrence was measured in dependence on the exit angle β with respect to the mirror surface. The experiment allowed also for a measurement of the speed and the charge of the scatter particle (see Fig. 3).

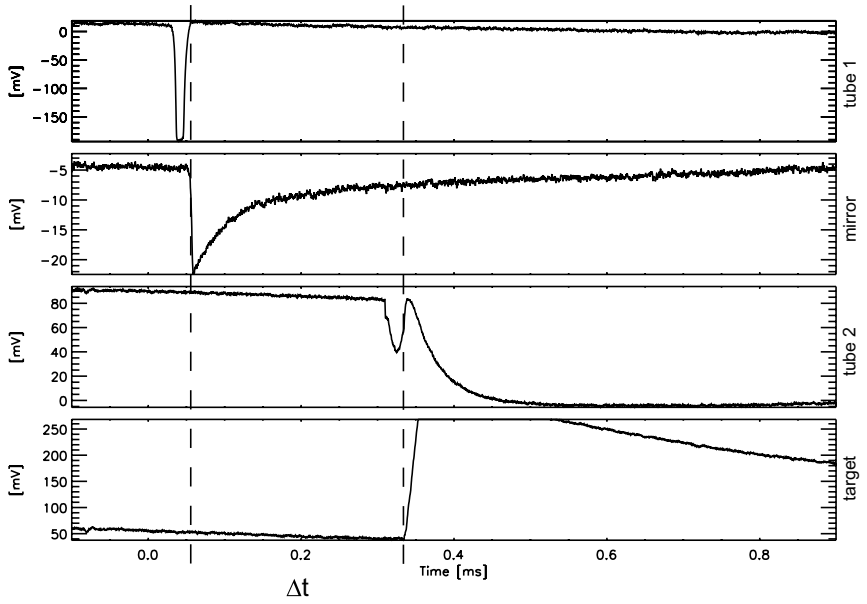

Figure 3. Signals obtained from the four detection units of the experiment shown in Fig. 2. The first oscilloscope curve (top panel) shows that the dust particle carrying a positive charge, passes through the first tube in the scatter chamber. The next curve (2.top panel) we see the impinging dust particle in the signal of the mirror. The following curve below shows the signal of a scatter particle with a much smaller positive charge, travelling through the second tube. The last curve (bottom panel) reveals the impact of the scatter particle on the target which was biassed with +35 V. The generated and attracted negative charges caused the huge signal, while the positive ions attracted by the nearby second tube gave rise to the relatively slowly emerging signal of opposite sign. The speed of the scatter particle is calculated by the ratio of the distance from mirror to target and the difference in time between the two signals which is indicated in the figure by the two dashed lines.

2.2.2 Damage to a wafer surface by scatter particles and their residues

The experimental set-up was similar to the one described in section 2.2.1 but the second tube and the target were replaced by a plain semiconductor wafer. The used silicon and germanium wafers had been polished to facilitate the locating of scatter particle impacts on the surface.

Three different measurements had been carried out with this set-up. At first wafers have been exposed directly to the iron dust particles. Then a series of measurements with new wafers has been carried out with dust particles impinging on the mirror under grazing incidence but no optical filter was placed in front of the wafers. And finally the test series was repeated again with new wafers and an optical filter was inserted in front of the wafer to reproduce the set-up of the pn-CCD camera.

The wafer surface was analyzed afterwards with a scanning electron microscope (SEM) in conjunction with an energy dispersive X-ray analysis (EDX). The EDX measurement enabled a search for chemical element residues of the scatter particles to identify their origin.

The EDX-spectrum of a silicon sample is dominated by the Si-K_α-line (1739 eV). The energy of that line is fairly close to the energy of the Al-K_α-line (1486 eV) so that it could be hard to resolve a weakly excited Al-K_α-line at the rising edge of the Si-K_α-peak in the EDX-spectrum. However, aluminum is of interest in the analysis because it is a characteristic component of the optical filter. For that reason germanium wafers have been used in addition. The Al-K_α-peak is almost equally close to the Ge-L_α-line (1188 eV) as to the Si-K_α-line but located at the better determined trailing edge.

2.2.3 The damage to a pn-CCD detector and the scatter particle distribution

Behind the tube and the mirror a 3 cm x 1 cm large pn-CCD detector was placed. It is of the same type as one of the units of the 2 x 6 pn-CCD array in the X-ray camera aboard XMM-Newton. The detector was cooled and fully operated during the test. The detector images were continuously recorded before, during and after a projectile hit the mirror. No event threshold was set so that the signal of each individual pixel of an image is stored for offline analysis. In front of the pn-CCD the optical filter was inserted to have the same configuration as in the flight camera.

With this experiment we could test whether scatter particles can cause bright pixels in the pn-CCD and compare the damage with the pn-CCD damage on XMM-Newton. The experiment with the pn-CCD should finally determine the number of scatter particles created by a single dust particle and their spatial and angular distribution. With the pn-CCD at the dust accelerator we covered a scatter angle range of 0.3º in vertical and 1.0º in the horizontal direction. According to the larger focal length of the Wolter telescope on XMM-Newton, the full 6 cm x 6 cm large CCD array corresponds to an angular range of about 0.5º.

3. ANALYSIS OF SCATTER PARTICLES

The measurement results obtained with the experimental set-up described above are presented in the following. The same sequence as for the experiment description is used.

3.1 Incidence, speed and charge of scatter particles

The probability for scatter particle occurrence at a scatter angle β was studied for four different grazing incidence angles α. The angles of 1.0º and 4.0º were tested with the 0.88º large aperture. Afterwards the angles of 1.5º and 2.0º were studied more accurately with a smaller angular aperture of 0.44º. The target position, expressed by the exit angle β, is defined with respect to the mirror. For example, a target at the angular position $\beta = 0^\circ$ is oriented perpendicular to the mirror surface and particles which hit the target are scattered off almost parallel to the mirror.

The speed of the dust particles was selected by means of the PSU in the range between 4.5 km/s and 5.5 km/s. A test series comprised 50 or 100 valid shots referring to particles that passed through the first tube at the entrance of the scatter chamber and hit onto the mirror.

A scatter particle event is registered if the signal of the copper target showed a particle impact whereas the tube in front of it indicates no particle impingement. The tube may show an induced signal of the passing through particle but not necessarily because this depends on the amount of electric charge on the scatter particle.

The analysis of the test series showed that high speed micron-sized particles impinging under grazing incidence on X-ray mirror surfaces produce scatter particles leaving the mirror under small angles. The results are summarized in Table 1. A high probability of at least 50% was measured for the occurrence of scatter particles at each of the four grazing incidence angles. The particles are scattered in forward direction, mostly under very small angles β close to 0^o which means almost parallel to the mirror surface. But also scatter angles of more than 0.5^o were observed. The frequency of scatter particles dropped rapidly with increasing exit angle. Turning the target to small negative angles results in a decreasing hit quota down to zero. This confirms the alignment of the set-up because the target is then shadowed by the mirror.

The analysis of the speed showed that the scatter particle had almost the same velocity as the incident dust projectile. This result agrees with hydrocode simulations about grazing hypervelocity impacts performed by ESA.[8] The simulations showed that the iron dust particle is deflected from the mirror. Its speed component parallel to the mirror surface is basically unchanged while the component normal to the mirror is strongly reduced after the impact. The reason for this is the absorption of the kinetic energy associated with the normal velocity component by a plastic deformation of the projectile. For that reason only small scatter angles occur typically.

The scatter particles appeared mostly as uncharged, but sometimes a positive charge could be detected (see Fig. 3). However the amount of total charge was much smaller than that of the primary dust particle.

3.2 SEM images and EDX analysis

Several polished wafers were exposed to primary dust particle impacts and to avoid ambiguities we accumulated scatter particle impacts on other wafers. The silicon wafers had a nitride layer with a thickness of 150 nm on top, while the germanium wafers were not processed at all. The dust accelerator had been operated for these measurements in continuous mode to improve the statistics. We had chosen a grazing incidence angle of 2^o for the iron dust impinging on the mirror surface. Afterwards SEM images were taken from the wafer surfaces. We detected craters in the silicon and germanium with different sizes and depths in the order of 0.1 μm up to 10 μm. A comparison of the craters caused by dust and by scatter particle impacts revealed no fundamental difference in shape and size (see Fig. 4).

An EDX analysis was performed in particular in the craters to search for residues of the scatter particles. The EDX spectra revealed at several locations the three iron lines: Fe-L- (0.7 keV), Fe-K_α-(6.4 keV) and Fe-K_β (7.1 keV). No obvious gold (Au-M_α-line at 2.1 keV) or aluminum lines (Al-K-line at 1.5 keV) could be detected in the spectra (Fig. 5).

In the analysis of the silicon samples two other lines were present all over the surface: a small N-peak at an energy of 0.4 keV due to the nitride layer and a dominanting Si-K-line at 1.7 keV. In some measurements an additional line at 3.5 keV was detected which could be identified as the pile-up of Si-K-X-rays. In germanium the same is valid for the three X-ray fluorescence lines of the substrate material: Ge-L (1.2 keV), Ge-K_α (9.9 keV) and Ge-K_β (11.0 keV).

We conclude from these results that the craters are caused by the iron dust particles or their large fragments scattered off the mirror surface onto the wafer. A forward ejection of gold particles from the mirror or of parts from the optical filter could is excluded at large significance.

grazing incidence angle α	scatter angle β	angular range $\Delta\beta$	target hits*
1.0º	-0.5º	[-0.94º; -0.06º]	0%
1.0º	**0.0º**	**[-0.44º; 0.44º]**	**80%**
1.0º	0.5º	[0.06º; 0.94º]	10%
1.0º	1.0º	[0.56º; 1.44º]	4%
1.5º	-0.25º	[-0.47º; -0.03º]	0%
1.5º	**0.00º**	**[-0.22º; 0.22º]**	**58%**
1.5º	0.13º	[-0.09º; 0.35º]	28%
1.5º	0.25º	[0.03º; 0.47º]	1%
2.0º	-0.2º	[-0.42º; 0.02º]	0%
2.0º	-0.1º	[-0.32º; 0.12º]	16%
2.0º	0.0º	[-0.22º; 0.22º]	32%
2.0º	**0.1º**	**[-0.12º; 0.32º]**	**50%**
2.0º	0.2º	[-0.02º; 0.42º]	40%
2.0º	0.4º	[0.18º; 0.62º]	2%
4.0º	-0.4º	[-0.84º; 0.04º]	6%
4.0º	**0.0º**	**[-0.44º; 0.44º]**	**80%**
4.0º	0.5º	[0.06º; 0.94º]	76%
4.0º	1.0º	[0.56º; 1.44º]	5%
4.0º	1.5º	[1.06º; 1.94º]	2%
4.0º	2.3º	[1.86º; 2.74º]	0%
4.0º	3.0º	[2.56º; 3.44º]	0%
4.0º	4.0º	[3.56º; 4.44º]	0%

* referring to 100% of valid shots, i.e. tube 1 and mirror signals o.k.

Table 1. Probabilities for scatter particle occurrence in dependence on the grazing incidence angle α of the dust particles and the scatter angle β with respect to the mirror. The entries which correspond to the highest hit quota are written in boldface.

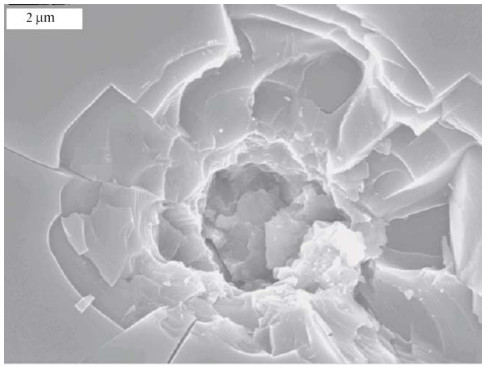

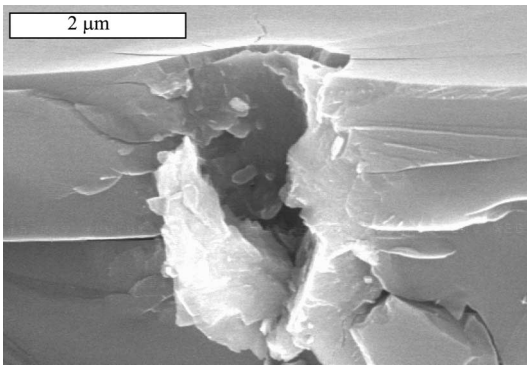

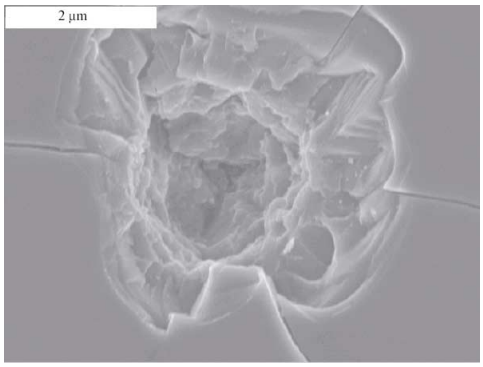

Figure 4. SEM images of craters in silicon after particle impacts. The SEM image top left shows the top view of a crater caused by a scatter particle.

A cross break of a silicon sample with a crater, again due to a scatter particle, is displayed in the side view image top right.

The damage caused by a primary dust particle is shown for comparison in the image bottom left.

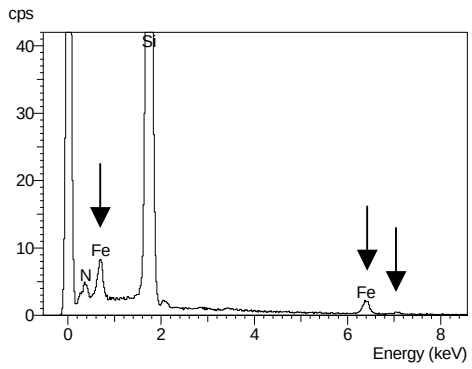

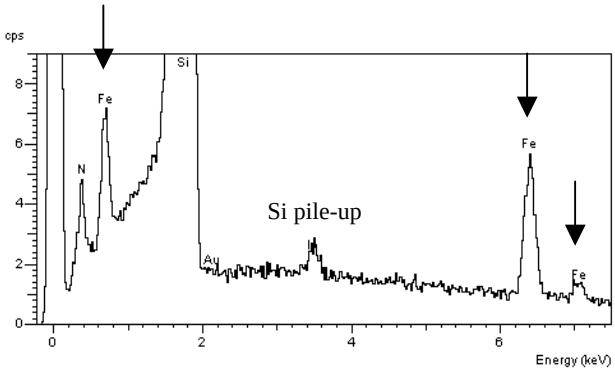

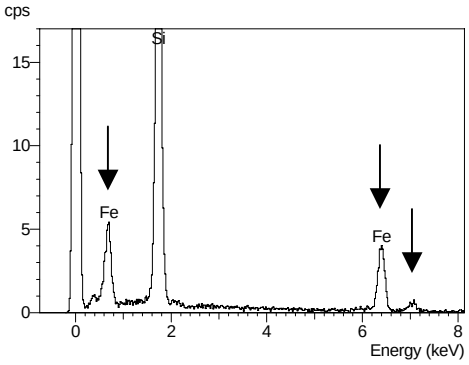

Figure 5. EDX spectra of craters in silicon. The top panel two spectra are for scatter particle impacts. The spectrum at the lower left is measured in a crater caused by a primary iron particle. The characteristic Fe-L-(0.7 keV), Fe-K_α-(6.4 keV) and Fe-K_β-lines (7.1 keV) are clearly visible, but no Au-M_α-line (2.1 keV) or Al-K-line (1.5 keV). The Fe residues are obviously due to the scattered dust particle, whereas no evidence exists that particles from the mirror surface or from the optical filter have come to rest in the crater. The N- and Si-lines come from top Si_3N_4-layer.

3.3 Analysis of pn-CCD damage created by scatter particles

In a first test a fully operated and cooled 3 cm x 1 cm large pn-CCD was exposed to primary dust particles. The effect to the pn-CCD was the lightening up of a single bright pixel per shot. However a heavily damaged pixel affects the sensitivity of all pixels in the transfer channel by an increase of their noise. The number of shots was thereby limited. The damage experiment was therefore performed with three pn-CCDs in total.

Dust particles hitting the mirror surface under grazing incidence created 1 bright pixel in most cases and up to about 20 pixels per shot. The bright pixels were simultaneously generated and distributed over up to 6 different locations on the detector area with maximum separation of more than 10 arcmin (Fig. 6). The maximum dark current of bright pixels was higher than 10^{-13} A at an operating temperature of -90ºC. In the frame where the impact of the scatter particles occurred, an energy distribution was observed with maximum values coinciding with the locations of the brightest pixels (Fig. 7). This effect, above referred to as "light flash", is predominantly due to the emission of infrared radiation. The transformation of the kinetic energy of the particles to heat results locally in an extremely high temperature.

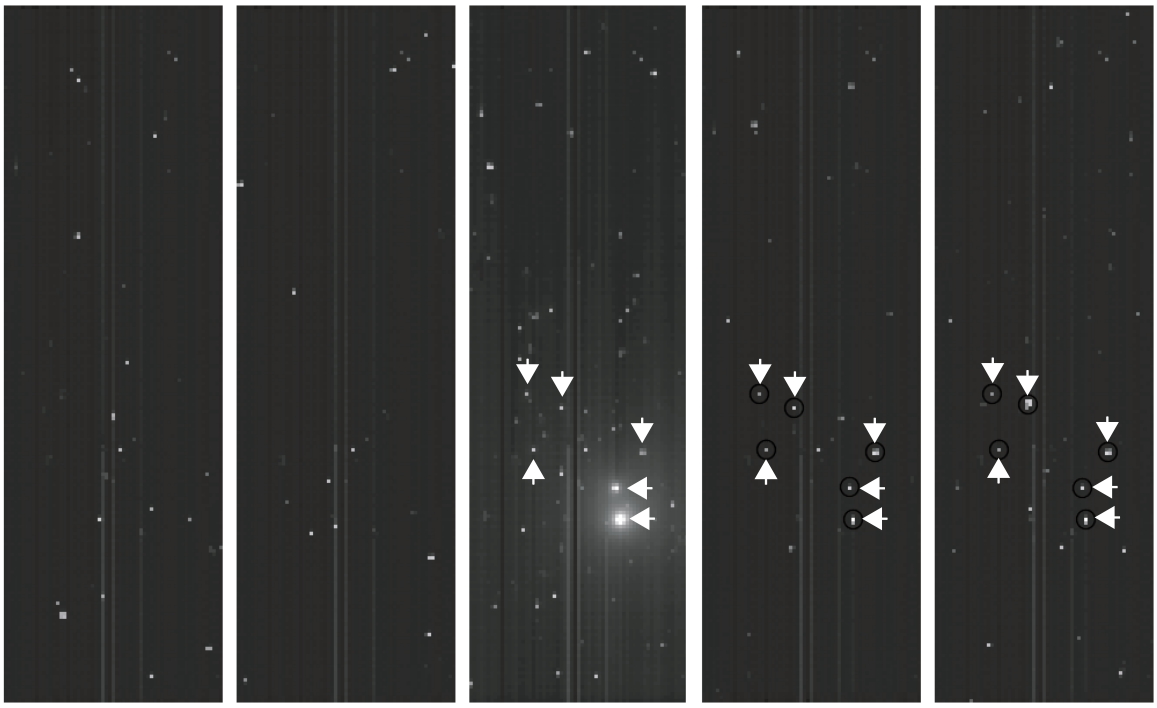

Figure 6. The picture shows a complete series of 5 successive pn-CCD frames (each lasting 44 ms) before, during and after the impacts of scatter particles in the experiment at the dust accelerator. The simultaneous impacts at 6 different locations in frame # 11779 were accompanied by a radiation flash with the highest intensity around the bright pixels. This event is caused by a single dust particle impinging under grazing incidence on the X-ray mirror. As a result of the impact about 20 bright pixels were generated. All frames appear noisy because of the damage due to prior impacts and due to X-rays and ions emitted from the dust accelerator during that time.

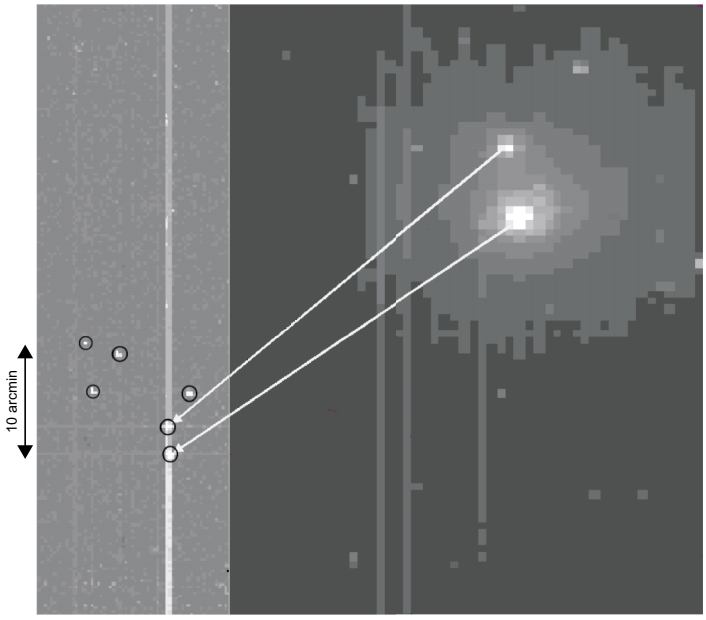

Figure 7. The left hand section of the picture shows the change of the pn-CCD dark image caused by the scatter products of a single dust particle impinging on the mirror (compare Fig. 6). The differential image has been gained from 200 images before and after the damage. At the position where the two most severely damaged pixel areas are located, the entire transfer channel became noisy. The bright pixels are distributed over a region of more than 10 arcmin.

The picture on the right hand side displays a zoom of the single frame #11779, i.e. at the time of the scatter particle impact. The maxima of the energy distribution coincide with the locations of the two most severely damaged pixels.

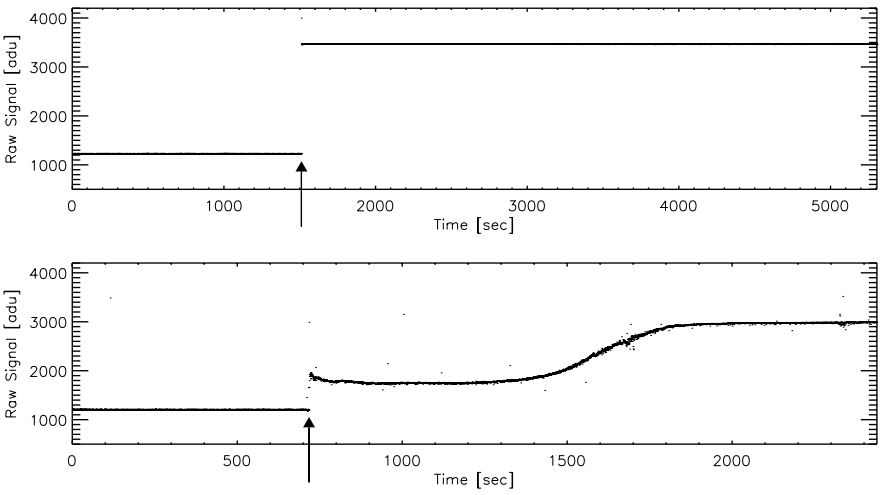

Figure 8. The curves show the dark current signal vs. time for two different types of bright pixels.

The plot of the upper panel illustrates that the dark current is immediately stable after the particle impact marked by an arrow.

The current in the other type of bright pixel is stable at first, increases then slowly with time and becomes finally constant (lower panel).

In summary, we conclude that the damage which occurred to the pn-CCD camera on XMM-Newton could be reproduced in the laboratory.

An analysis of the charge generation rate as a function of time revealed two different types of bright pixels, shown in Fig. 8. The first type shows a constant generation rate immediately after the particle impact. For the second type we observe after the first lightening up of the bright pixels a slow increase of the generation current until the current becomes finally stable. This agrees with our observation of the behavior of some bright pixels after the event aboard XMM-Newton had occurred.

4. SUMMARY AND CONCLUSIONS

The experiments at the dust accelerator verified that a dust particle impinging under grazing incidence on an X-ray mirror can cause a damage as observed in the focal plane CCD-detectors aboard XMM-Newton. All the characteristics of the event and the damage could be reproduced in the laboratory. The formation of the bright pixels is caused by fragments of the primary dust particle.

Micrometeoroids in space may be more fragile and have higher speeds than the compact iron particles of the dust accelerator. Furthermore a multiple interaction of the micrometeorid and its fragments with Wolter-I telescope surfaces is likely to happen before they can reach the detector. This increases the probability that micrometeoroids break up and a shower of scatter particles occurs.

In the case of the XMM-Newton mission one micrometeorid event per more than 30 months and camera happened. The generated bright pixels cover less than 0.03% of the sensitive pn-CCD area. However the statistics is too poor for further solid predictions.

For future X-ray missions like XEUS, a study about the probability of micrometeoroid events is mandatory. The large collection area of the mirrors enhances the problem, but the small solid angle due to the large focal length is favorably. Finally the different orbit compared with XMM-Newton has to be taken into account for an estimate of the micrometeoroid damage rate.

ACKNOWLEDGMENTS

The authors would like to thank Gerhard Schäfer and Sebastian Kuhn of the Max-Planck-Institut für Kernphsik in Heidelberg for their support at the dust accelerator.

REFERENCES

1. F. Jansen, D. Lumb, B. Altieri, J. Clavel et al., "XMM-Newton observatory, I.The spacecraft and operations", *Astronomy&Astrophysics*, vol.365, 1, pp. L1-L6, 2001.
2. N. Meidinger, H. Bräuninger, U. Briel, R. Hartmann et al., "The PN-CCD detector for XMM and ABRIXAS", *Proc. SPIE* 3765, pp.192-203, 1999.
3. L. Strüder, U. Briel, K. Dennerl, R. Hartmann et al., "The European Photon Imaging Camera on XMM-Newton: The pn-CCD camera", *Astronomy&Astrophysics*, vol.365, 1, pp. L18-L26, 2001.
4. K. Dennerl, U.G. Briel, M. Freyberg, F. Haberl, N. Meidinger, and V.E. Zavlin, "CTI History of the EPIC PN Camera", *Proc. Symposium New Visions of the X-ray Universe in the XMM-Newton and Chandra Era*, ed. F. Jansen, ESA SP-488, 2002
5. L. Strüder, B. Aschenbach, H. Bräuninger, G. Drolshagen et al., "Evidence for micrometeoroid damage in the pn-CCD camera system aboard XMM-Newton", *Astronomy&Astrophysics*, vol.375, pp. L5-L8, 2001.
6. B. Altieri, XMM-Newton Science Operations Centre, Vilspa, ESA, P. Bennie, Physics & Astronomy Dept., University of Leicester, E. Serpell, ESOC, private communication.
7. M. Stübig, G. Schäfer, T. Ho, R. Srama, and E. Grün, "Laboratory simulation improvements for hypervelocity micrometeorite impacts with a new dust particle source", *Planetary and Space Science*, vol.49, pp. 853-858, 2001.
8. D. Palmieri, "Grazing hypervelocity impacts simulation on the XMM-Newton mirrors", *working paper*, ref. EWP-2175, ESTEC, ESA, 2002.